Structural Eng./Earthquake Eng., JSCE, Vol. 15, No. 2, 175s—190s, 1998 July
(J. Struct. Mech. Earthquake Eng., JSCE, No. 598/ I —44)

A STUDY OF MODE COUPLING IN FLUTTER AND BUFFETING OF THE AKASHI-KAIKYO BRIDGE

Hiroshi KATSUCHI[1], Nicholas P. JONES[2], Robert H. SCANLAN[3] and Haruki AKIYAMA[4]

[1] Member of JSCE, M.S., Research Associate, Dept. of Civil Engineering, Yokohama National University (79-5, Tokiwadai, Hodogaya-ku, Yokohama 240-8501, Japan)
[2,3] Ph.D., Professor, Dept. of Civil Engineering, The Johns Hopkins University (3400 N. Charles St., Baltimore, MD 21218, USA)
[4] Member of JSCE, Ph.D., General Manager, Mukaishima Construction Office, Honshu-Shikoku Bridge Authority (5890-1, Mukaishima-cho, Mitsugi-gun, Hiroshima 722-0073, Japan)

Flutter and buffeting of the Akashi-Kaikyo Bridge were analyzed using a newly developed analytical tool, which is able to consider fully aeroelastic and aerodynamic coupling effects among modes. The analysis well demonstrated the behavior of a wind-tunnel model and particularly could capture the mode-coupling effects. Six primary modes dominated the flutter of the Akashi-Kaikyo Bridge where significant mode couplings of the 1st torsional mode with three vertical modes were observed. The multi-mode analysis also provided insights into the coupling mechanism in buffeting in which strong aeroelastic and aerodynamic interactions between vertical and torsional modes were observed.

***Key Words**: Akashi-Kaikyo Bridge, flutter, buffeting, multi-mode analysis, mode coupling*

1. INTRODUCTION

Wind-resistant design is one of the key factors in the realization of long-span bridges. As the span length increases, aeroelastic phenomena (vortex shedding, galloping, divergence, flutter and buffeting) must be carefully considered in the design stage. Wind-tunnel testing has been widely used for that purpose since the Tacoma Narrows Bridge collapse in 1940.

Recently, analytical prediction methods aided by progress in computer technology are more commonly used. These methods are typically represented as flutter and buffeting analyses in which parameters in the analysis are experimentally obtained. The analytical methods have great advantages of flexibility, saving time and cost, and of yielding a great deal of insight into the physics of the aeroelastic phenomena.

Multi-mode-analysis approaches[1)-7)] have been proposed in the last decade by several researchers. These predicted the possible mode coupling in the flutter and buffeting of long-span bridges, in particular, Jain et al.[7)] presented several examples of the possibility of aeroelastic and aerodynamic coupling among modes. Further, the Honshu-Shikoku Bridge Authority performed a wind-tunnel test using a 40-meter-long aeroelastic model of the Akashi-Kaikyo Bridge, and observed significant mode coupling in the flutter state[1)].

This paper first analytically demonstrates the flutter and buffeting of the wind-tunnel model of the Akashi-Kaikyo Bridge, then discusses mode-coupling effects, and finally provides insights into the mechanisms of mode coupling in the flutter and buffeting.

Miyata et al.[1)] investigated the fact that six primary modes were coupled in the flutter of the Akashi-Kaikyo Bridge, and lateral flutter derivatives P_i^* (i = 2, 3, 5 and 6) played a significant role in the flutter onset. However, there still seem to remain issues to be investigated, e.g., to what extent each of the six modes participated in the flutter, and what is the nature of the coupling mechanism at flutter? In addition, buffeting analysis has been usually performed in Japan neglecting aerodynamic and aeroelastic mode coupling for analytical brevity. However, since significant mode coupling was experimentally observed in the flutter of the Akashi-Kaikyo Bridge, mode coupling in buffeting

must also be expected.

The analytical procedure used in this study was developed by Jain et al.[7),8)], implementing the theory of Scanlan and Jones[9)], and is able to capture the fully coupled aeroelastic and aerodynamic response of long-span bridges to wind excitation.

Therefore, with this analytical tool, it is of great interest to investigate the mode-coupling effects and mechanisms in the flutter and buffeting of the Akashi-Kaikyo Bridge, particularly buffeting, which has not been fully analyzed in a multi-mode sense before.

2. GENERAL FORMULATION

The analytical method used here is based on a modal analysis in the frequency domain[7)-9)]. This is summarized here for context. In a modal analysis, the deflection components of the bridge deck are represented in terms of the generalized coordinate of the mode $\xi_i(t)$, the deck width B and the dimensionless modal values of the i^{th} mode along the deck $h_i(x)$, $p_i(x)$ and $\alpha_i(x)$ as

$$\text{vertical: } h(x,t)=\sum_i h_i(x)B\xi_i(t) \tag{1a}$$

$$\text{lateral: } p(x,t)=\sum_i p_i(x)B\xi_i(t) \tag{1b}$$

$$\text{torsion: } \alpha(x,t)=\sum_i \alpha_i(x)\xi_i(t) \tag{1c}$$

where x is the coordinate along the deck span and t is time.

The governing equation of motion of ξ_i is

$$I_i[\ddot{\xi}_i+2\zeta_i\omega_i\dot{\xi}_i+\omega_i^2\xi_i]=q_i(t) \tag{2}$$

where I_i and $q_i(t)$ are the generalized inertia and force of the i^{th} mode, and ζ_i and ω_i are the damping ratio-to-critical and the circular natural frequency of the i^{th} mode, respectively.

The generalized force $q_i(t)$ is defined by

$$q_i(t)=\int_0^l[Lh_iB+Dp_iB+M\alpha_i]dx \tag{3}$$

where l is deck span length and L, D and M represent the lift, drag and pitching moment per unit span length . The lift, drag and pitching moment per unit span are defined by

$$\text{lift:} \quad L = L_{ae} + L_b \tag{4a}$$

$$\text{drag:} \quad D = D_{ae} + D_b \tag{4b}$$

$$\text{moment:} \quad M = M_{ae} + M_b \tag{4c}$$

where the subscripts *ae* and *b* refer to aeroelastic and buffeting, respectively.

For purely sinusoidal motions of frequency ω, the aeroelastic forces can be expressed as

$$L_{ae}=\frac{1}{2}\rho U^2B\left[KH_1^*\frac{\dot{h}}{U}+KH_2^*\frac{B\dot{\alpha}}{U}+K^2H_3^*\alpha+K^2H_4^*\frac{h}{B}+KH_5^*\frac{\dot{p}}{U}+K^2H_6^*\frac{p}{B}\right] \tag{5a}$$

$$D_{ae}=\frac{1}{2}\rho U^2B\left[KP_1^*\frac{\dot{p}}{U}+KP_2^*\frac{B\dot{\alpha}}{U}+K^2P_3^*\alpha+K^2P_4^*\frac{p}{B}+KP_5^*\frac{\dot{h}}{U}+K^2P_6^*\frac{h}{B}\right] \tag{5b}$$

$$M_{ae}=\frac{1}{2}\rho U^2B^2\left[KA_1^*\frac{\dot{h}}{U}+KA_2^*\frac{B\dot{\alpha}}{U}+K^2A_3^*\alpha+K^2A_4^*\frac{h}{B}+KA_5^*\frac{\dot{p}}{U}+K^2A_6^*\frac{p}{B}\right] \tag{5c}$$

where ρ is the air density, U is the mean wind speed, $K(=B\omega/U)$ is the reduced frequency and H_i^*, P_i^* and A_i^*, i = 1 - 6 are the flutter derivatives of the deck cross section.

Under assumed slowly varying gust action, the buffeting forces are defined as

$$L_b=\frac{1}{2}\rho U^2B\left[C_L(2\frac{u}{U})+(C_L'+C_D)\frac{w}{U}\right]=\frac{1}{2}\rho U^2B\mathbf{L}_b(x,t) \tag{6a}$$

$$D_b=\frac{1}{2}\rho U^2B\left[C_D(2\frac{u}{U})+C_D'\frac{w}{U}\right]=\frac{1}{2}\rho U^2B\mathbf{D}_b(x,t) \tag{6b}$$

$$M_b=\frac{1}{2}\rho U^2B^2\left[C_M(2\frac{u}{U})+C_M'\frac{w}{U}\right]=\frac{1}{2}\rho U^2B^2\mathbf{M}_b(x,t) \tag{6c}$$

where C_L, C_D and C_M are the static lift, drag and pitching moment coefficients (referred to deck width B) of a typical deck cross section, respectively, $C_L' = dC_L/d\alpha$, $C_D' = dC_D/d\alpha$ and $C_M' = dC_M/d\alpha$, and $u = u(t)$, $w = w(t)$ are the along-wind and vertical velocity fluctuations of the wind, respectively.

The multi-mode system of equations can be expressed in matrix notation as

$$\mathbf{I}\xi''+\mathbf{A}\xi'+\mathbf{B}\xi=\mathbf{Q}_b(s) \tag{7}$$

where ξ = generalized coordinate vector, ( )' represents a derivative with respect to dimensionless time $s = Ut/B$ (which is introduced for analytical convenience) **I** is an identity matrix, **A, B** are the damping, stiffness matrices of the system, respectively, and $\mathbf{Q}_b$ is the generalized force vector.

At this point, if it is expected that the flutter derivatives along a span vary due to the change of

angle of attack and geometric condition of the deck, the general terms of **A**, **B** and $\mathbf{Q}_b$ are expressed as

$$\mathbf{A}_{ij}(K) = 2\zeta_i K_i \delta_{ij} - \frac{\rho B^4 l K}{2I_i}[G^{H_1^*}_{h_i h_j} + G^{H_2^*}_{h_i \alpha_j} + G^{H_5^*}_{h_i p_j} + G^{P_1^*}_{p_i p_j} + G^{P_2^*}_{p_i \alpha_j} + G^{P_5^*}_{p_i h_j} + G^{A_1^*}_{\alpha_i h_j} + G^{A_2^*}_{\alpha_i \alpha_j} + G^{A_5^*}_{\alpha_i p_j}] \quad (8)$$

$$\mathbf{B}_{ij}(K) = K_i^2 \delta_{ij} - \frac{\rho B^4 l K^2}{2I_i}[G^{H_3^*}_{h_i \alpha_j} + G^{H_4^*}_{h_i h_j} + G^{H_6^*}_{h_i p_j} + G^{P_3^*}_{p_i \alpha_j} + G^{P_4^*}_{p_i p_j} + G^{P_6^*}_{p_i h_j} + G^{A_3^*}_{\alpha_i \alpha_j} + G^{A_4^*}_{\alpha_i h_j} + G^{A_6^*}_{\alpha_i p_j}] \quad (9)$$

$$\mathbf{Q}_{b_i}(s) = \frac{\rho B^4 l}{2I_i}\int_0^l \{\mathbf{L}_b(x,s)h_i + \mathbf{D}_b(x,s)p_i + \mathbf{M}_b(x,s)\alpha_i\}\frac{dx}{l} \quad (10)$$

where δ_{ij} (= 1 when $i = j$, otherwise = 0) is the Kronecker delta, and $K_i = B\omega_i / U$. The modal integrals ($G^{T_m^*}_{r_i s_j}$) are obtained by

$$G^{T_m^*}_{r_i s_j} = \int_0^l T_m^*(x) r_i(x) s_j(x) \frac{dx}{l} \quad (11)$$

where T_m^* = H_m^*, P_m^* or A_m^* (m = 1,..,6), r_i = h_i , p_i or α_i , and s_j = h_j , p_j or α_j. Note that the spanwise coordinate x locates information about the type of cross section and the angle of attack.

The diagonal terms ($i = j$) in (8) and (9) represent the single-degree-of-freedom (and uncoupled) equations while the off-diagonal terms introduce the aeroelastic coupling through the flutter derivatives and the mechanical coupling through the cross-modal integrals among different modes.

Defining the Fourier transform of $f(s)$ to be

$$\overline{f}(K) = \int_0^\infty f(s) e^{-iKs} ds \quad (12)$$

and taking the Fourier transform of (7) yields the new system of equations in the reduced frequency(K) domain such that

$$\mathbf{E}\overline{\xi} = \overline{\mathbf{Q}}_b \quad (13)$$

where

$$\mathbf{E}_{ij} = -K^2 \delta_{ij} + iK\mathbf{A}_{ij}(K) + \mathbf{B}_{ij}(K) \quad (14)$$

and $i = \sqrt{-1}$.

(1) Identification of flutter condition

The flutter condition is identified by solving the aeroelastically influenced eigenvalue problem

$$\mathbf{E}\overline{\xi} = \mathbf{0} \quad (15)$$

In order to obtain a nontrivial solution for (15), the determinant of matrix **E** must vanish. Additionally, since the matrix **E** is complex, the condition of det**E** = 0 must be satisfied requiring that both the real and imaginary parts of the determinant are simultaneously zero[10]. This can be accomplished by fixing a value of K and seeking a value of ω, in the frequency range of interest, for which the determinant is zero; and then repeating this process, changing the value of K, until both determinants are zero at the same ω. At this point, the flutter frequency is obtained from ω and the flutter speed can be calculated from K (= $\omega B/U$) and ω.

For a multi-mode problem, the same procedures are required as many times as the number of modes and the highest solution of K of all solutions gives the flutter-critical condition. The mode corresponding to the solution of ω is the dominant mode in the flutter condition. Moreover, the eigenvector ξ at the flutter condition gives the "flutter mode shape" which indicates the relative participation of each structural mode in flutter.

(2) Analytical procedure for buffeting

The vector of buffeting forces on the right hand side of (13) is

$$\overline{\mathbf{Q}}_b = \frac{\rho B^4 l}{2}\begin{Bmatrix} \frac{1}{I_1}\int_0^l \overline{\mathbf{F}}_{b_1}\frac{dx}{l} \\ \frac{1}{I_2}\int_0^l \overline{\mathbf{F}}_{b_2}\frac{dx}{l} \\ \vdots \\ \frac{1}{I_n}\int_0^l \overline{\mathbf{F}}_{b_n}\frac{dx}{l} \end{Bmatrix} \quad (16)$$

where the integrands in the vector above are

$$\overline{\mathbf{F}}_{b_i}(x,K) = \overline{\mathbf{L}}_b(x,K)h_i(x) + \overline{\mathbf{D}}_b(x,K)p_i(x) + \overline{\mathbf{M}}_b(x,K)\alpha_i(x) \quad (17)$$

Substituting for the terms above from appropriately transformed (6a) - (6c) at span location x_A leads to

$$\overline{\mathbf{F}}_{b_i}(x_A,K) = \frac{1}{U}[\{2C_L h_i(x_A) + 2C_D p_i(x_A) + 2C_M \alpha_i(x_A)\}\overline{u}(K) + \{(C_L' + C_D)h_i(x_A) + C_D' p_i(x_A) + C_M' \alpha_i(x_A)\}\overline{w}(K)] \quad (18)$$

A complex conjugation operation (denoted by the asterisk) for $\overline{\mathbf{Q}}_b$ gives the following equation as

$$\overline{\mathbf{Q}}_b \overline{\mathbf{Q}}_b^{*T} = \left(\frac{\rho B^4 l}{2}\right)^2 \times \begin{bmatrix} \ddots & & \vdots & & \iddots \\ & \ddots & \vdots & \iddots & \\ \cdots & \cdots & \frac{1}{I_i I_j}\int_0^l\int_0^l \overline{\mathbf{F}}_{b_i}\overline{\mathbf{F}}_{b_j}^* \frac{dx_A}{l}\frac{dx_B}{l} & \cdots & \cdots \\ & \iddots & \vdots & \ddots & \\ \iddots & & \vdots & & \ddots \end{bmatrix} \quad (19)$$

from which the power spectral density (PSD) matrix

can be developed.

A general term of the PSD matrix is

$$S_{Q_{h_i}Q_{h_j}}(K)=\left(\frac{\rho B^4 l}{2U}\right)^2 \times\frac{1}{l_i l_j}\int_0^l\int_0^l\{\tilde{q}_i(x_A)\tilde{q}_j(x_B)S_{uu}(x_A,x_B,K) +\tilde{r}_i(x_A)\tilde{r}_j(x_B)S_{ww}(x_A,x_B,K)+[\tilde{q}_i(x_A)\tilde{r}_j(x_B) +\tilde{r}_i(x_A)\tilde{q}_j(x_B)]C_{uw}(x_A,x_B,K)+i[\tilde{q}_i(x_A)\tilde{r}_j(x_B) -\tilde{r}_i(x_A)\tilde{q}_j(x_B)]Q_{uw}(x_A,x_B,K)\}\frac{dx_A}{l}\frac{dx_B}{l} \quad (20)$$

where

$$\tilde{q}_i(x)=2[C_L h_i(x)+C_D p_i(x)+C_M\alpha_i(x)] \quad (21)$$

$$\tilde{r}_j(x)=(C_L'+C_D)h_j(x)+C_D' p_j(x)+C_M'\alpha_j(x) \quad (22)$$

S_{uu} and S_{ww} are spanwise cross-spectral densities of u and w components, respectively, and C_{uw} and Q_{uw} are spanwise uw-cospectral- and quadrature-spectral densities, respectively.

The spanwise auto- and cross-spectral densities of the wind components are defined here referring to Roberts and Surry[11] and the measurement in the wind-tunnel testing[12] as

$$S_{uu}(x_A,x_B,K)=S_{uu}(K)R_{uu}(x_A,x_B,K) =S_{uu}(K)\exp\left\{-\frac{cB_1}{2\pi}\frac{|x_A-x_B|}{L_3}\sqrt{1+70.8\left(\frac{KL_3}{2\pi B}\right)^2}\right\} \quad (23)$$

$$S_{ww}(x_A,x_B,K)=S_{ww}(K)R_{ww}(x_A,x_B,K) =S_{ww}(K)\exp\left\{-\frac{cB_1}{2\pi}\frac{|x_A-x_B|}{L_4}\sqrt{1+70.8\left(\frac{KL_4}{2\pi B}\right)^2}\right\} \quad (24)$$

$$C_{uw}(x_A,x_B,K)=C_{uw}(K)R_{uw}(x_A,x_B,K) =C_{uw}(K)\sqrt{R_{uu}(x_A,x_B,K)\cdot R_{ww}(x_A,x_B,K)} \quad (25)$$

where $S_{uu}(K)$ and $S_{ww}(K)$ are auto-power spectral densities of u- and w-velocity fluctuations, respectively, $C_{uw}(K)$ is a co-spectral density of the uw-cross spectrum, c (= 8) is the decay factor, and equivalent turbulence scales L_3 (= 70 m) and L_4 (= 40 m) are determined based on the measurements[12] in the wind-tunnel testing. Q_{uw} was not included in this analysis because there was no quantitative assessment available and its contribution is considered to be relatively small.

An aerodynamic admittance, a function of K defining the correlation between the section wind speed fluctuation and the developed wind force, was taken as the Davenport formula for drag and unity for lift and pitching moment based on the measurements[13].

$$\text{drag: } |\chi_D(K)|^2=\left\{\frac{2}{(cK')^2}[cK'-1+\exp(-cK')]\right\} \quad (26)$$

lift and pitching moment:

$$|\chi_L(K)|^2=|\chi_M(K)|^2=1 \quad (27)$$

where $K'=DK/2\pi B$, D is the deck height.

There is an argument in buffeting analysis that the spanwise coherence of buffeting forces is larger than that of wind-speed fluctuations. In this study, both were assumed to be same. That is, the spanwise coherence of wind-speed fluctuations was defined based on measurements in the wind-tunnel test, and that of buffeting forces was given via aerodynamic admittance. Ultimately, it is desirable that this issue should be dealt with along with aerodynamic admittance in order to elucidate buffeting mechanisms in long-span bridges.

Using the following expression as

$$H_{r_i s_j}^{T_{mn}}(K)=\int_0^l\int_0^l r_i(x_A)s_j(x_B)R_{mn}(x_A,x_B,K)\frac{dx_A}{l}\frac{dx_B}{l} \quad (28)$$

where r_i and $s_i = h_i$, p_i or α_i, m and $n = u$ or w, and $T = C$ or S according to mn, the ij^{th} term of the buffeting force matrix can be expressed as

$$S_{Q_{h_i}Q_{h_j}}(K)=\left(\frac{\rho B^4 l}{2U}\right)^2\frac{1}{l_i l_j}\left[Y_{ij}^{S_{uu}}(K)S_{uu}(K) +Y_{ij}^{S_{ww}}(K)S_{ww}(K)+Y_{ij}^{C_{uw}}(K)C_{uw}(K)\right] \quad (29)$$

where

$$Y_{ij}^{S_{uu}}(K)=(2C_L|\chi_L|)^2 H_{h_i h_j}^{S_{uu}}+(2C_D|\chi_D|)^2 H_{p_i p_j}^{S_{uu}} +(2C_M|\chi_M|)^2 H_{\alpha_i\alpha_j}^{S_{uu}}+4C_L C_D(\chi_L\chi_D^* H_{h_i p_j}^{S_{uu}} +\chi_D\chi_L^* H_{p_i h_j}^{S_{uu}})+4C_L C_M(\chi_L\chi_M^* H_{h_i\alpha_j}^{S_{uu}}+\chi_M\chi_L^* H_{\alpha_i h_j}^{S_{uu}}) +4C_D C_M(\chi_D\chi_M^* H_{p_i\alpha_j}^{S_{uu}}+\chi_M\chi_D^* H_{\alpha_i p_j}^{S_{uu}}) \quad (30)$$

$$Y_{ij}^{S_{ww}}(K)=((C_L'+C_D)|\chi_L|)^2 H_{h_i h_j}^{S_{ww}}+(C_D'|\chi_D|)^2 H_{p_i p_j}^{S_{ww}} +(C_M'|\chi_D|)^2 H_{\alpha_i\alpha_j}^{S_{ww}}+(C_L'+C_D)C_D'(\chi_L\chi_D^* H_{h_i p_j}^{S_{ww}} +\chi_D\chi_L^* H_{p_i h_j}^{S_{ww}})+(C_L'+C_D)C_M'(\chi_L\chi_M^* H_{h_i\alpha_j}^{S_{ww}} +\chi_M\chi_L^* H_{\alpha_i h_j}^{S_{ww}})+C_D'C_M'(\chi_D\chi_M^* H_{p_i\alpha_j}^{S_{ww}}+\chi_M\chi_D^* H_{\alpha_i p_j}^{S_{ww}}) \quad (31)$$

$$Y_{ij}^{C_{uw}}(K)=2\{2(C_L'+C_D)C_L|\chi_L|^2 H_{h_i h_j}^{C_{uw}} +2C_D C_D'|\chi_D|^2 H_{p_i p_j}^{C_{uw}}+2C_M C_M'|\chi_M|^2 H_{\alpha_i\alpha_j}^{C_{uw}}+[C_L C_D' +(C_L'+C_D)C_D](\chi_L\chi_D^* H_{h_i p_j}^{C_{uw}}+\chi_D\chi_L^* H_{p_i h_j}^{C_{uw}})+[C_L C_M' +(C_L'+C_D)C_M](\chi_L\chi_M^* H_{h_i\alpha_j}^{C_{uw}}+\chi_M\chi_L^* H_{\alpha_i h_j}^{C_{uw}})+(C_D C_M' +C_D' C_M)(\chi_D\chi_M^* H_{p_i\alpha_j}^{C_{uw}}+\chi_M\chi_D^* H_{\alpha_i p_j}^{C_{uw}})\} \quad (32)$$

and the asterisks denote complex conjugates.

For the Akashi-Kaikyo Bridge, $S_{uu}(K)$ and $S_{ww}(K)$ were modeled using the Hino spectrum and Bush and Panofsky spectrum, respectively, based on the measurements[12] in the wind-tunnel testing.

$$S_{uu}(K) = 0.4751 \frac{u^2}{\beta} \left\{ 1 + \left(\frac{K}{2\pi\beta} \frac{U}{B} \right)^2 \right\}^{-5/6}$$

$$\beta = 0.01718 \frac{\alpha K_r U_{10}}{I_u{}^3} \left(\frac{z}{10} \right)^{(2m-3)\alpha-1} \quad (33)$$

$$S_{ww}(K) = 0.632 w^2 \frac{z / f_{\max}}{U[1+1.5(Kz / 2\pi B f_{\max})^{5/3}]} \quad (34)$$

where α (= 1/8) is the exponent of wind velocity profile, K_r (= 0.0025) is the surface friction coefficient, m is a modification factor for the spectrum shape associated with turbulence scale, U_{10} (= 46.0 m/s) is the design reference wind speed at 10 m above sea level and z is the elevation. The modification factor m in the analysis was set to 3 and f_{max} = 0.4 based on the measurements[12] in the wind tunnel.

Since there are no measurements for the actual Akashi-Kaikyo Bridge as yet, an empirical formula for C_{uw} was used[14].

$$C_{uw}(K) = -\frac{14 z u_*^2}{U[1+9.6(Kz / 2\pi B)]^{2.4}} \quad (35)$$

where u_* is the surface friction velocity.

The power spectral density matrix for the generalized coordinate ξ is developed using (13) as

$$\mathbf{S}_{\xi\xi}(K) = \mathbf{E}^{-1} \mathbf{S}_{Q_b Q_b} [\mathbf{E}^*]^{-1} \quad (36)$$

where $\mathbf{E}^*$ is the complex conjugate transpose of matrix $\mathbf{E}$.

The PSD of the physical displacements for (1a) - (1c) can be obtained from the PSD of the respective generalized displacement components through

$$S_{hh}(x_A, x_B, K) = \sum_i \sum_j B^2 h_i(x_A) h_j(x_B) S_{\xi_i \xi_j}(K) \quad (37)$$

$$S_{pp}(x_A, x_B, K) = \sum_i \sum_j B^2 p_i(x_A) p_j(x_B) S_{\xi_i \xi_j}(K) \quad (38)$$

$$S_{\alpha\alpha}(x_A, x_B, K) = \sum_i \sum_j \alpha_i(x_A) \alpha_j(x_B) S_{\xi_i \xi_j}(K) \quad (39)$$

where i and j represent the summation over the number of modes being used in the analysis.

Evaluation of the spectral densities of the displacements at combinations of discrete x_A and x_B will result in a matrix. The mean-square values of these displacements can be evaluated in terms of their respective PSD functions

$$\sigma_h^2(x_A, x_B) = \int_0^\infty S_{hh}(x_A, x_B, f) df \quad (40)$$

$$\sigma_p^2(x_A, x_B) = \int_0^\infty S_{pp}(x_A, x_B, f) df \quad (41)$$

$$\sigma_\alpha^2(x_A, x_B) = \int_0^\infty S_{\alpha\alpha}(x_A, x_B, f) df \quad (42)$$

where f is the frequency. Covariance matrices for h, p and α are thus obtained, from which statistics of the displacement components h, p and α can be calculated.

Neglecting any coupling terms among modes results in a single-mode buffeting calculation. Based on the formulations developed above, the PSD of the physical displacements at a specific point x, for the single-mode buffeting, $S_{h_i}(x, K)$, $S_{p_i}(x, K)$ and $S_{\alpha_i}(x, K)$ can be obtained by the same procedures as those in the multi-mode buffeting.

Then the mean-square values of these displacements can be evaluated as

$$\sigma_{q_i}^2(x) = \int_0^\infty S_{q_i}(x, f) df \quad (43)$$

where $q_i = h_i$, p_i or α_i.

For the purpose of evaluating the response in the multi-mode sense from single-mode responses, the square-root of the sum of square (SRSS) of single-mode responses method is used, i.e.:

$$\mathrm{SRSS}(x) = \sqrt{\sigma_{q_1}^2(x) + \sigma_{q_2}^2(x) + \cdots\cdots + \sigma_{q_n}^2(x)} \quad (44)$$

where n is the number of modes.

3. FLUTTER ANALYSIS

(1) Description of analysis

Flutter derivatives of the deck used here, which were measured[15] by a forced vibration method in a smooth flow, were components of H_1^*,.., H_4^*, A_1^*,.., A_4^*, P_2^*, P_3^*, P_5^* and P_6^*. P_1^* was estimated using quasi-steady theory as[16]

$$P_1^* = -2C_D/K \quad (45)$$

The flutter derivatives in the analysis were given as a function of angle of attack, which is also a function of span location, since it is associated with deck rotation due to the wind loading. In addition, two different sets of flutter derivatives, which were measured using deck-section models with different main cable heights, were applied to the 340-meter-long section at the span center where main cables were close to the deck and affected deck stability aerodynamically[17].

(2) Flutter analysis of wind-tunnel model

Flutter analyses predicted the behavior of the wind-tunnel model of the Akashi-Kaikyo Bridge, as

Table 1 Flutter speeds and frequencies of analysis and measurement

Cross Section & Flow Angle: α_w (deg.)	Flutter Speed (m/s) Analysis	Measurement	Flutter Frequency (Hz) Analysis	Measurement
Original, $\alpha_w = 0$	79.1 [*78.8*]	84.0	0.146	0.135
Original, $\alpha_w = +2.7$	79.8 [*82.0*]	85.0	0.148	0.136
Modified, $\alpha_w = 0$	81.3 [*82.9*]	90.0	0.148	0.140
Modified, $\alpha_w = +2.7$	91.9 [*90.0*]	96.0	0.146	N.A.
Partially Modified, $\alpha_w = 0$	80.0 [*82.8*]	90.0	0.148	N.A.
Partially Modified, $\alpha_w = +2.7$	91.4 [*91.6*]	N.A.	0.146	N.A.

Flutter speeds in [ ] were obtained by another analysis[1]. N.A.: not available

Table 2 Eigenvectors of **E** at flutter

(a) Magnitude: $|\overline{\xi_i}|$

	Original		Modified		Partially Modified	
	$\alpha_w = 0$	+2.7 deg.	$\alpha_w = 0$	+2.7 deg.	$\alpha_w = 0$	+2.7 deg.
Mode 1	6.847E-02	2.884E-02	5.649E-02	4.636E-02	5.457E-02	4.306E-02
Mode 2	2.447E-01	2.238E-01	2.020E-01	2.449E-01	1.987E-01	2.593E-01
Mode 10	2.241E-01	1.816E-01	1.713E-01	1.546E-01	1.587E-01	1.540E-01
Mode 11	6.383E-02	5.604E-02	7.754E-02	1.069E-01	7.483E-02	1.005E-01
Mode 12	1.000E+00	1.000E+00	1.000E+00	1.000E+00	1.000E+00	1.000E+00
Mode 13	2.438E-01	2.238E-01	1.770E-01	1.844E-01	1.653E-01	1.894E-01

(b) Phase: $\tan^{-1}(I_m/R_e)$ where R_e and I_m are the real and imaginary part of $\overline{\xi_i}$ vector, respectively.

	Original		Modified		Partially Modified	
	$\alpha_w = 0$	+2.7 deg.	$\alpha_w = 0$	+2.7 deg.	$\alpha_w = 0$	+2.7 deg.
Mode 1	-172.0	-178.1	-166.7	-167.7	-166.8	-167.8
Mode 2	18.0	24.0	22.6	24.5	23.2	25.0
Mode 10	-162.5	-157.9	-160.7	-153.6	-162.9	-153.1
Mode 11	17.4	-6.9	6.0	8.1	5.0	6.6
Mode 12	0.0	0.0	0.0	0.0	0.0	0.0
Mode 13	-17.1	-7.6	-5.3	-5.3	-8.3	-7.2

shown in **Tables 1** and **2**, and **Fig. 1**. Flutter stability of the Akashi-Kaikyo Bridge was secured by installing a stabilizing device just below an open slot on the road deck center, which is a vertical thin plate enhancing air stream through the slot, consequently diminishing the difference in air pressure between locations above and below the deck. The modified cross section includes this device while the original does not. The partially modified case consists of the modified section in the center span and the original section in both side spans. Flutter derivatives in each case were chosen accordingly.

Based on a previous study[1], six primary symmetric modes; 1st lateral (mode 1), 1st vertical (mode 2), 2nd vertical (mode 10), 2nd lateral (mode 11), 1st torsion (mode 12) and 3rd vertical (mode 13) were used in all the analyses. **Fig. 1** shows the real and imaginary roots of det**E** = 0 for the original and modified cross sections with α_w = 0 deg. The intersection of the real and imaginary roots gives flutter onset and the corresponding mode to the intersection is a dominant mode to flutter. Mode 12 (1st symmetric torsion) was the leading mode in all six cases in **Tables 1** and **2**.

All of the flutter speeds calculated in this study are lower (4% - 11%) than those measured in the wind-tunnel testing, but are in good agreement with those analyzed in the previous study[1], as seen in **Table 1**. This suggests that the analysis in this study appears reliable and consistent. One reason for these differences in the flutter speeds between the analysis and measurement may be due to an existing effective reduction in the spatial correlation of flutter derivatives (aeroelastic forces) in the physical model. Its effect can be taken[18), 19)] into (11) in the same manner as the spanwise coherence of buffeting forces in (28), however it was not considered in this analysis.

The analyses showed that the flutter of the Akashi-

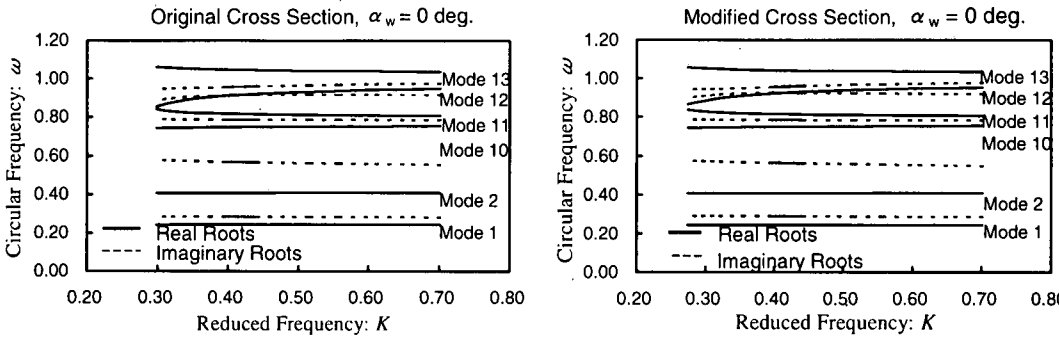

Fig. 1 Real and imaginary roots of det**E** = 0 in flutter analysis

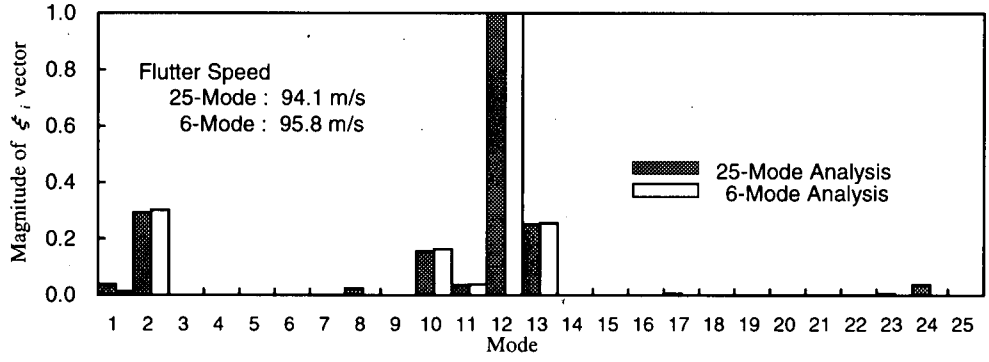

Fig. 2 Comparison of mode participation between 25- and 6-mode analyses

Table 3 Mode participation ($\left|\overline{\xi_i}\right|$) of six primary modes to flutter

Case	Mode						Flutter Speed (m/s)
	1	2	10	11	12	13	
1	0.0685	0.2447	0.2241	0.0638	1.0	0.2438	79.1
2	—	0.2558	0.2173	0.0686	1.0	0.2340	80.4
3	0.1461	—	0.3416	0.1650	1.0	0.2785	96.1
4	0.0848	0.2818	—	0.0862	1.0	0.2467	84.2
5	0.0733	0.2577	0.2174	—	1.0	0.2353	81.0
6	N.D.	N.D.	N.D.	N.D.	—	N.D.	> 135
7	0.0540	0.2142	0.1734	0.0480	1.0	—	73.9
8	—	0.2699	—	—	1.0	—	82.0
9	—	0.2328	0.1914	—	1.0	—	76.3
10	—	0.2233	0.1827	0.0497	1.0	—	74.9

N.D.: not determined.

Kaikyo Bridge was multi-mode coupled flutter in which one torsional (mode 12), three vertical modes (modes 2, 10 and 13) with the relatively small participation of two lateral modes (modes 1 and 11) were coupled. However, there are no significant differences among the eigenvectors at flutter among the analytical cases.

(3) Modal contributions

In order to investigate the possibility that any other modes than the six modes identified above participated in the flutter, a flutter analysis with the first 25 modes of the Akashi-Kaikyo Bridge was performed. The flutter speed in the 25-mode analysis drops by about 2% from that of the six-

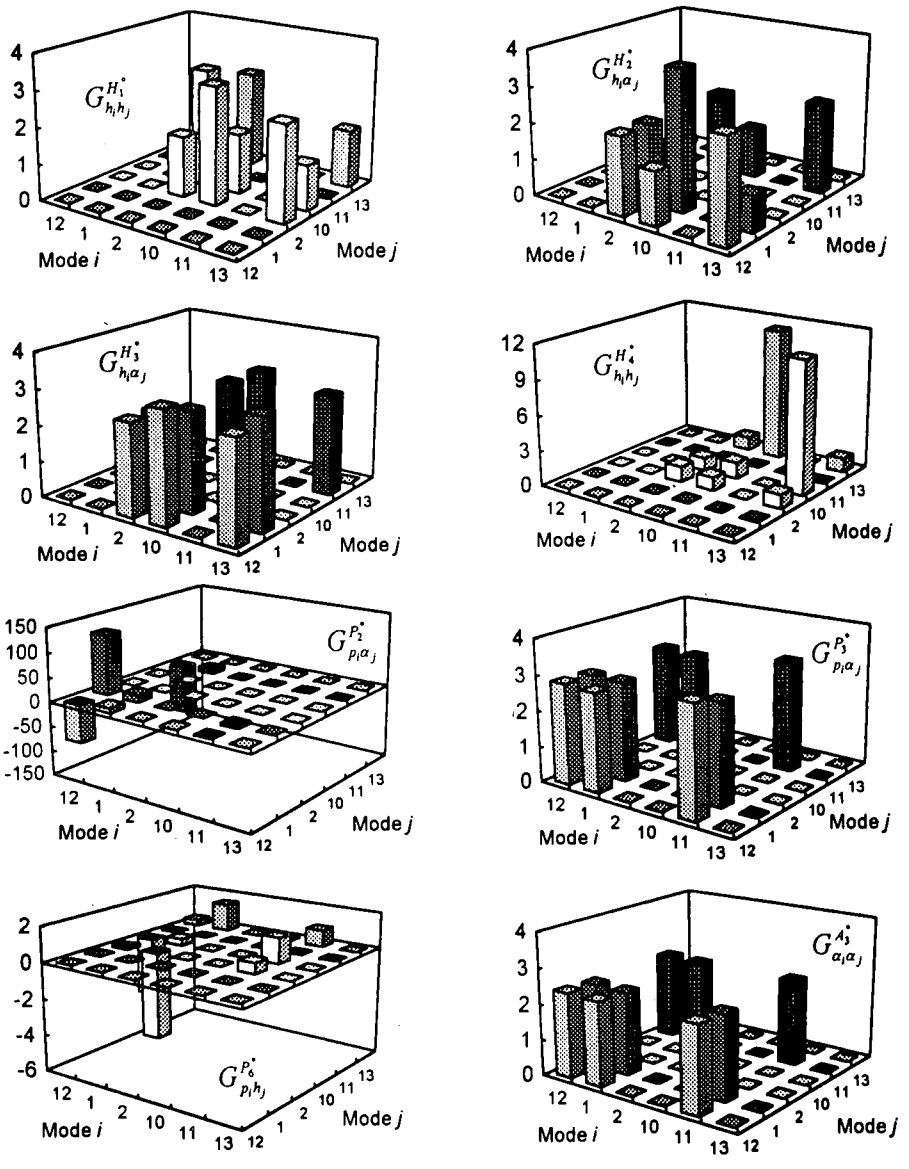

Fig. 3 Evolution ratio of components in G-integral terms between flutter onset and 48 m/s

mode analysis and the six primary modes are dominant in the 25-mode analysis, as shown in **Fig. 2.** Modes 8 and 24 with relatively large contributions are a longitudinal and a cable lateral mode, respectively.

In addition, the extent to which each of the six modes contributed to flutter was investigated. Flutter analyses with different combinations of the six modes were performed as shown in **Table 3**. The contribution of modes 1 and 11 are small and mode 12 is essential for the flutter, that is, flutter did not occur in a case in which mode 12 was excluded. However flutter ultimately occurred otherwise even when mode 2 was excluded.

Concerning the flutter speed, it is noteworthy that even the two-mode (modes 2 and 12) case (classical theory) gave a result very close to the six-mode case. However, flutter mode in the two-mode case was considerably different, in particular in vertical and lateral components, from that in the six-mode case. Modes 10 and 11 played a destabilizing role (low flutter speed) while mode 13 stabilized the system (high flutter speed), which is consistent with the buffeting analysis presented later. It is also noteworthy that no significant differences in the eigenvectors can be seen among different mode combinations except Case 3.

(4) Coupling mechanism

It has been determined so far that several modes were coupled in the flutter of the Akashi-Kaikyo Bridge. In this Section, the underlying mechanism of the multi-mode coupled flutter of the Akashi-Kaikyo Bridge is investigated.

The coupling among modes is achieved through aerodynamic and aeroelastic interactions, both of which depend on flutter derivatives and on vibration mode shapes. These interactions are taken into account in the flutter analysis by (8) and (9). Therefore, observation of the values of the G-integral terms defined by (11) before and after flutter onset will provide the information on the coupling mechanism among modes. In this study, using the six-mode analysis for the original cross section with $\alpha_w = 0$ deg., the G-integral term values were obtained at flutter condition onset and at a wind speed of 48 m/s, which was far from flutter.

Fig. 3 shows the ratio of these values between the flutter speed and 48 m/s. Shown are G-integral terms whose components changed significantly (magnitude changed by more than factor of two). No significant components were observed in other G-integral terms. Since the effect of modes 1 and 11 on flutter was small as described in the previous section, and so was that of P_6^* [20], omitting components associated with these modes and the flutter derivative from **Fig. 3** will provide the essential information. Then, dividing the significant components remaining into two groups corresponding to $\mathbf{A}_{ij}$ and $\mathbf{B}_{ij}$ will conclude that $G^{H_1^*}_{h_2h_{10}}$, $G^{H_1^*}_{h_2h_{13}}$, $G^{H_1^*}_{h_{10}h_2}$, $G^{H_1^*}_{h_{13}h_2}$, $G^{H_2^*}_{h_2\alpha_{12}}$, $G^{P_{21}^*}_{p_{12}\alpha_{12}}$ and $G^{H_2^*}_{h_{13}\alpha_{12}}$ in $\mathbf{A}_{ij}$, and $G^{H_3^*}_{h_2\alpha_{12}}$, $G^{H_3^*}_{h_{10}\alpha_{12}}$, $G^{H_4^*}_{h_{10}h_{13}}$, $G^{A_3^*}_{\alpha_{12}\alpha_{12}}$, $G^{P_{31}^*}_{p_{12}\alpha_{12}}$, $G^{H_4^*}_{h_{13}\alpha_{10}}$ and $G^{H_3^*}_{h_{13}\alpha_{12}}$ in $\mathbf{B}_{ij}$ evolved significantly between flutter and 48 m/s.

It follows from above that mode combinations in which significance was observed are (2-10), (2-12), (2-13), (10-2), (12-12), (13-2) and (13-12) in $\mathbf{A}_{ij}$, and (2-12), (10-12), (10-13), (12-12), (13-10) and (13-12) in $\mathbf{B}_{ij}$. It can also be said that these mode combinations provide strong mode couplings at flutter onset. Strong mode couplings are recognized in a diagonal component of mode 12 (1st torsion) and off-diagonal components between modes 2, 10 or 13 (1st, 2nd or 3rd vertical, respectively) and mode 12. Strong mode couplings are also recognized in off-diagonal components among these three vertical modes. This may be related to the fact that the flutter of the Akashi-Kaikyo Bridge was a bending-torsion coupled type and mode 12 was a dominant mode.

Flutter derivatives producing the strong mode couplings are H_1^*, H_2^* and P_2^* in $\mathbf{A}_{ij}$, and H_3^*, H_4^*, P_3^* and A_3^* in $\mathbf{B}_{ij}$. In particular, H_2^* and P_2^* in $\mathbf{A}_{ij}$, and H_3^* and P_3^* in $\mathbf{B}_{ij}$ are coupled terms. It is thought that these terms played an important role in the coupled flutter of the Akashi-Kaikyo Bridge. Actually, it was pointed out[20] that P_2^* and P_3^* greatly contributed to flutter onset and destabilized the system. In addition, Matsumoto[21] concluded that H_3^* was one of the components significantly contributing to coupled flutter of long-span bridges.

Table 4 Static coefficients of deck cross sections

Cross Section	C_L C_L'	C_D C_D'	C_M C_M'
Original $\alpha = 0$ deg.	0.09418 1.90460	0.38624 0.0	0.01038 0.27174
Modified $\alpha = 0$ deg.	0.02465 1.19175	0.42050 0.0	0.01317 0.30653

4. BUFFETING ANALYSIS

(1) Description of analysis

The first 17 vibration modes, with the exception of very low-contribution modes such as cable modes and longitudinal modes, were used here in the buffeting analysis. They were modes 1 to 7, 10 to 14, 22, 23 and 25 to 27. The components of the flutter derivatives used in the buffeting analysis were the same as those in the flutter analysis, that is, H_1^*,.., H_4^*, A_1^*,.., A_4^*, P_2^*, P_3^*, P_5^* and P_6^*. The flutter derivatives were interpolated well enough to capture the peaks associated with natural frequencies and were also carefully extrapolated so as to cover the frequency range which effectively contributes to the response[20]. P_1^* was estimated by quasi-steady theory from (45). Static coefficients of the deck cross section used in the buffeting analysis are listed in **Table 4**.

(2) Multi- and single-mode analysis

Single-mode RMS responses, which were represented as SRSS responses, and multi-mode RMS responses for the original and modified cross sections were calculated at wind speeds of 30 m/s, 60 m/s and 78 m/s, then compared with measurements[12] in the wind-tunnel testing. The wind speeds of 60 m/s and 78 m/s are the design wind speed of the deck and the minimum required flutter speed of the Akashi-Kaikyo Bridge, respectively. **Figs. 4** and **5** shows the comparisons of the RMS responses in the middle of the center span between the analyses and the measurements. The measurement data were evaluated as the average value of 15 sets of measurements. Their maximum and minimum values are also shown in

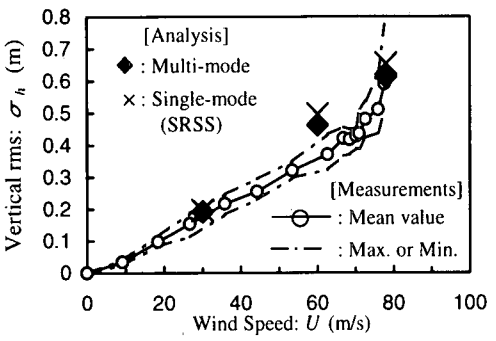

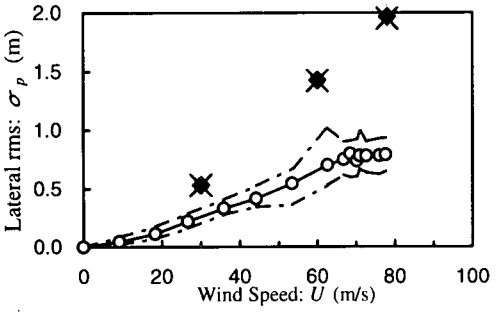

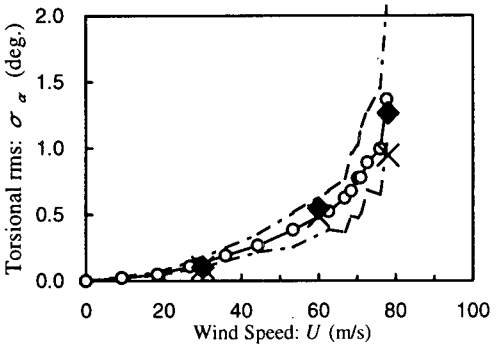

Fig. 4 Comparisons of RMS responses in original cross section between analyses and measurements

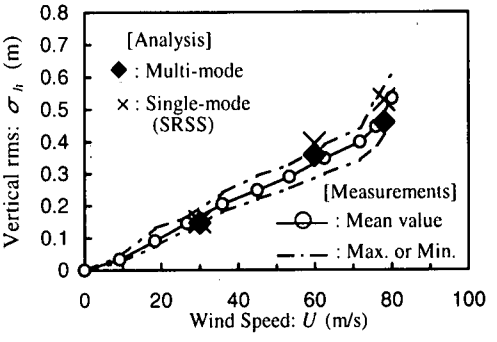

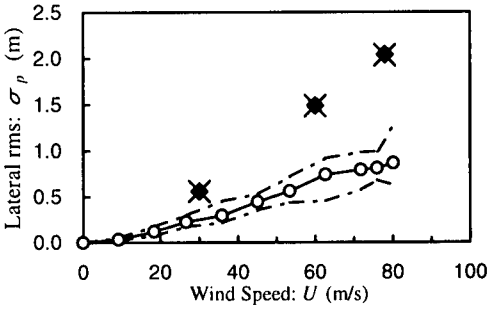

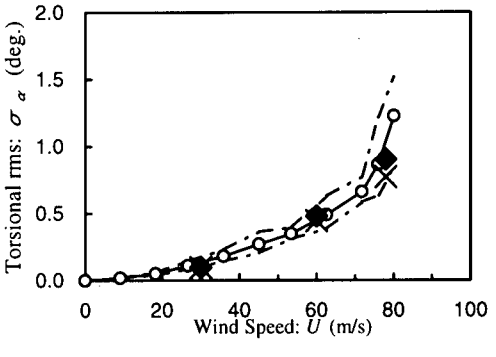

Fig. 5 Comparisons of RMS responses in modified cross section between analyses and measurements

the figures.

Good agreement can been seen between the multi-mode responses and the measurements in the vertical and torsional directions. In particular, the multi-mode analysis could well simulate the notable features of the measurements that the torsional response rapidly increased after 70 m/s, and that the difference of the torsional RMS between the multi-mode and single-mode analyses (and hence the coupling effects in the multi-mode calculation) become significant as the wind speed increased.

On the other hand, a difference of a factor of around 2 persisted in the lateral responses between the analyses; multi-mode and single-mode, and the measurement. In addition, no coupling effect can be seen in the lateral response of the multi-mode calculation. The analysis used all measurement data available such as PSD and spatial correlation of wind-speed fluctuations, static coefficients, and flutter derivatives. Besides, the effects of static deflection, lateral flutter derivatives (P_i^*, i = 2, 3, 5 and 6), both of which greatly affected flutter instability, and uw cospectrum C_{uw} on the buffeting were investigated, however those were not a possible solution for the discrepancy in the lateral buffeting[20]. The possible reasons for the discrepancy are suggested as estimation errors associated with P_1^* and the representation of aerodynamic admittance, but specific evidence has not been obtained[20] relative to this structure.

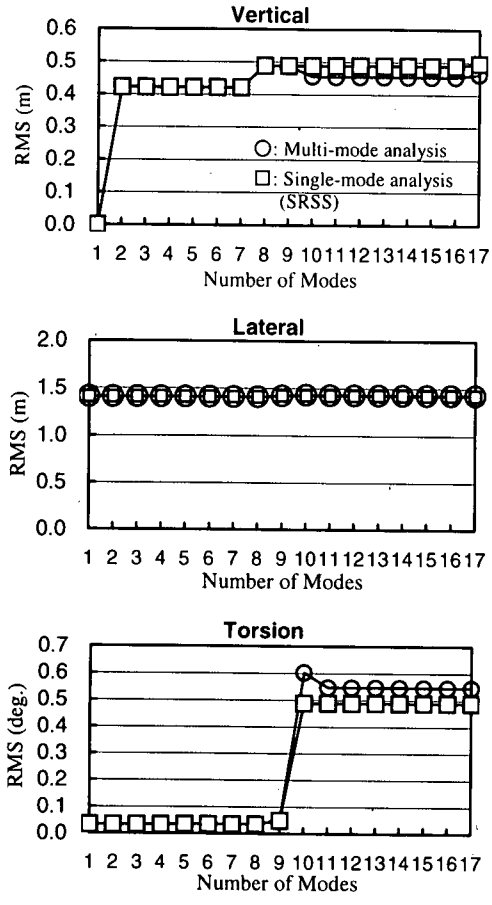

Fig. 6 Evolution of RMS response v.s. number of modes in original cross section

(3) Mode coupling in buffeting

In order to observe the mode-by-mode contribution to RMS response, buffeting analyses were performed changing the number of participating modes in the analysis.

Fig. 6 shows the evolution of the RMS responses of the original cross section versus the number of modes used in the analysis. All of these are from the multi-mode buffeting calculations at the wind speed of 60 m/s.

The RMS responses generally increased as the number of contributing modes increased, however there are two significant differences to be observed in the vertical and torsional directions. The vertical RMS decreased between the 9- and 10-mode analyses due to the addition of mode 12, and the torsional RMS also decreased between the 10- and 11-mode analyses due to the addition of mode 13.

These effects may be caused by mode coupling. That is, including mode 12 appears to shift the buffeting response into the torsion mode and including mode 13 also appears to shift the buffeting response into the vertical mode. This latter case is consistent with the fact that in the flutter analysis the flutter speed increased after the inclusion of mode 13.

Further investigations of these reductions of the RMS responses were performed for different wind-speed steps, 30 m/s and 78 m/s, and for the modified cross section, as shown in **Tables 5** and **6**. In the cases of wind speeds 30 m/s and 60 m/s in both cross sections, a similar mode-coupling effect can be seen as described above. In the case of 78 m/s, however, different coupling effects between the original and modified cross sections can be seen. In the original cross section, the vertical response increased a little in the 10-mode analysis, and the torsional responses greatly decreased in the 11-mode analysis. On the other hand, in the modified cross section, both vertical response in the 10-mode analysis and torsional response in the 11-mode analysis decreased, and its response-decreasing trends are consistent among the 3 wind-speed steps. That is, the response-decreasing ratios become large as the wind speed increases.

Based on the buffeting analysis theory, mode coupling information is collected into the PSD matrix for the generalized coordinate ξ, $\mathbf{S}_{\xi\xi}(K)$ in (36). In order to check the coupling effects in terms of the displacement, the covariance matrix of ξ, $\mathrm{COV}(\xi_i, \xi_j)$ was obtained by integrating $\mathbf{S}_{\xi\xi}(K)$ over frequency, i.e.,

$$\mathrm{COV}(\xi_i, \xi_j) = \int_0^\infty S_{\xi_i \xi_j}(f)\,df \qquad (46)$$

Figs. 7 and **8** show the differences in the COV matrices of the original and modified cross sections between 9- and 10-mode analyses [$\mathrm{COV}_{10}(\xi_i, \xi_j) - \mathrm{COV}_9(\xi_i, \xi_j)$], and between 10- and 11-mode analyses [$\mathrm{COV}_{11}(\xi_i, \xi_j) - \mathrm{COV}_{10}(\xi_i, \xi_j)$] at each wind-speed step (Note that the dimension of the COV matrices at each mode step is different).

Since physical displacements are obtained from the COV matrix through mode shapes, for example,

$$\sigma_h^2(x_A, x_B) = \sum_i \sum_j B^2 h_i(x_A) h_j(x_B) \mathrm{COV}(\xi_i, \xi_j) \qquad (47)$$

$$\sigma_\alpha^2(x_A, x_B) = \sum_i \sum_j \alpha_i(x_A) \alpha_j(x_B) \mathrm{COV}(\xi_i, \xi_j) \qquad (48)$$

and only vertical- and torsion-mode-related components in the COV matrix contribute to the vertical and torsional responses, respectively, reduction of $\mathrm{COV}(\xi_2, \xi_2)$ between the 9- and 10-mode analyses, and that of $\mathrm{COV}(\xi_{12}, \xi_{12})$ between the 10- and 11-mode analyses were identified as

Table 5 Multi-mode buffeting response of original cross section

		9-Mode Analysis	10-Mode Analysis	11-Mode Analysis
U = 30 m/s	σ_h [m]	0.1939 (1.000)	0.1901 (0.980)	—
	σ_α [deg.]	—	0.1028 (1.000)	0.1015 (0.987)
U = 60 m/s	σ_h [m]	0.4874 (1.000)	0.4552 (0.934)	—
	σ_α [deg.]	—	0.6020 (1.000)	0.5460 (0.907)
U = 78 m/s	σ_h [m]	0.6375 (1.000) [0.6385]	0.6439 (1.010) [0.6385]	—
	σ_α [deg.]	—	1.7178 (1.000) [0.9455]	1.2653 (0.737) [0.9455]
COV(ξ_i, ξ_j) at 78 m/s				
(i, j) = (2, 2)		0.2277E-03 (1.000)	0.1874E-03 (0.823)	—
(i, j) = (10, 2)		0.9782E-06 (1.000)	0.1924E-04 (19.67)	—
(i, j) = (10, 10)		0.9457E-04 (1.000)	0.1030E-03 (1.089)	—
(2,2) + (10,2) + (10,10)		0.3223E-03 (1.000)	0.3096E-03 (0.961)	
(i, j) = (12, 12)		—	0.8988E-03 (1.000)	0.4869E-03 (0.542)

Note: ( ) in the same rows are the ratios. [ ] are SRSS responses.

Table 6 Multi-mode buffeting response of modified cross section

		9-Mode Analysis	10-Mode Analysis	11-Mode Analysis
U = 30 m/s	σ_h [m]	0.1496 (1.000)	0.1455 (0.973)	—
	σ_α [deg.]	—	0.0980 (1.000)	0.0971 (0.991)
U = 60 m/s	σ_h [m]	0.3864 (1.000)	0.3503 (0.907)	—
	σ_α [deg.]	—	0.5048 (1.000)	0.4779 (0.947)
U = 78 m/s	σ_h [m]	0.5155 (1.000) [0.5172]	0.4555 (0.884) [0.5172]	—
	σ_α [deg.]	—	0.9908 (1.000) [0.7703]	0.9011 (0.909) [0.7703]
COV(ξ_i, ξ_j) at 78 m/s				
(i, j) = (2, 2)		0.1523E-03 (1.000)	0.9714E-04 (0.638)	—
(i, j) = (10, 2)		0.8957E-06 (1.000)	0.4554E-05 (5.084)	—
(i, j) = (10, 10)		0.5856E-04 (1.000)	0.5890E-04 (1.004)	—
(2,2) + (10,2) + (10,10)		0.2118E-03 (1.000)	0.1606E-03 (0.758)	—
(i, j) = (12, 12)		—	0.2972E-03 (1.000)	0.2456E-03 (0.826)

Note: ( ) in the same rows are the ratios. [ ] are SRSS responses.

primary factors in the reductions of the vertical and the torsional RMS, respectively. COV(ξ_2, ξ_2) and COV(ξ_{12}, ξ_{12}) are both diagonal terms related to modes 2 and 12, respectively.

Tables 5 and **6** also show the significant components in the corresponding COV matrices at the wind speed of 78 m/s. A significant difference between both cross sections at the wind speed of 78 m/s is in changes to the vertical components. COV (ξ_2, ξ_2) of both cross sections decreased by similar amounts while COV(ξ_{10}, ξ_{10}), diagonal term related to mode 10, of the original cross section increased by 9%. In addition, COV(ξ_{10}, ξ_2), the off-diagonal term related to modes 10 and 2, of the original cross section significantly increased. Even though COV (ξ_2, ξ_2) decreased for both cross sections, COV(ξ_{10}, ξ_2) and COV(ξ_{10}, ξ_{10}) increased and compensated for the reduction of COV(ξ_2, ξ_2) in the original cross section. This would be a reason why the vertical response of the original cross section at 78 m/s did not decrease between the 9- and 10-mode analyses as described earlier.

These mode-coupling mechanisms might be related to the flutter stability of the Akashi-Kaikyo Bridge. Under the assumption made in the buffeting analysis of no static deflection of the deck, it was estimated in a study[20] that flutter was about to occur at 78 m/s in the original section while the modified section was far from flutter at the same 78 m/s.

Since the Akashi-Kaikyo Bridge showed a coupled flutter, mode-coupling activity at 78 m/s must be higher in the original cross section than in the modified cross section. In fact, differences between the torsional responses in the modified cross section between the multi-mode analysis and

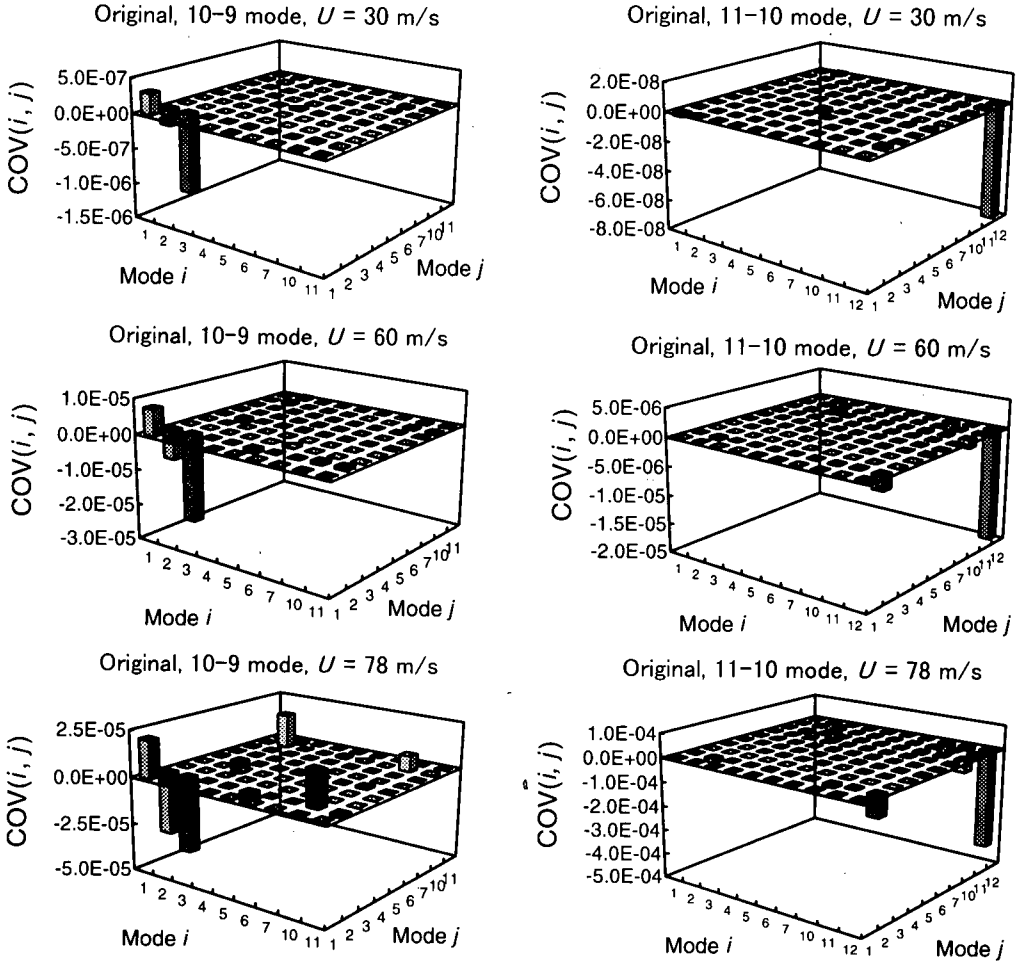

Fig. 7 Differences of COV matrices between 9- and 10-mode, and 10- and 11-mode analyses (Original cross section)

the SRSS responses, which were shown in brackets in **Tables 5** and **6**, are smaller than those in the original cross section. Therefore, this is thought to be a reason why many components in the COV matrix participated in the mode-coupling of the original cross section.

a) Parameter study

Finally, parameter studies on the reductions of $\mathrm{COV}(\xi_2, \xi_2)$ and $\mathrm{COV}(\xi_{12}, \xi_{12})$ in the COV matrices at the wind speed of 60 m/s were performed. Since a COV matrix was defined by $\mathbf{E}$ and $\mathbf{S}_{Q_hQ_h}$ (referring to (36) and (46)), it may be noted that the H-integrals (28) dominate the coupling conditions in $\mathbf{S}_{Q_hQ_h}$, and the G-integrals (11) and the associated flutter derivatives dominate the coupling conditions in $\mathbf{E}$.

Considering that vertical RMS decreased just after adding mode 12, effects of coupling components between modes 2 and 12 in the H- and G-integrals were investigated with the 10-mode analysis. Similarly, those between modes 12 and 13 were investigated with the 11-mode analysis in light of the fact that torsional RMS decreased just after adding mode 13. Six parameter analyses were performed for each case, as shown in **Table 7**.

If the responses obtained from the first of the parameter analyses for the 10-mode analysis, in which a parameter $G^{H_2^*}_{h_2\alpha_{12}}$ was equated to zero, recovered or approached those of the original 9-mode analysis in terms of σ_h and $\mathrm{COV}(\xi_2, \xi_2)$, the

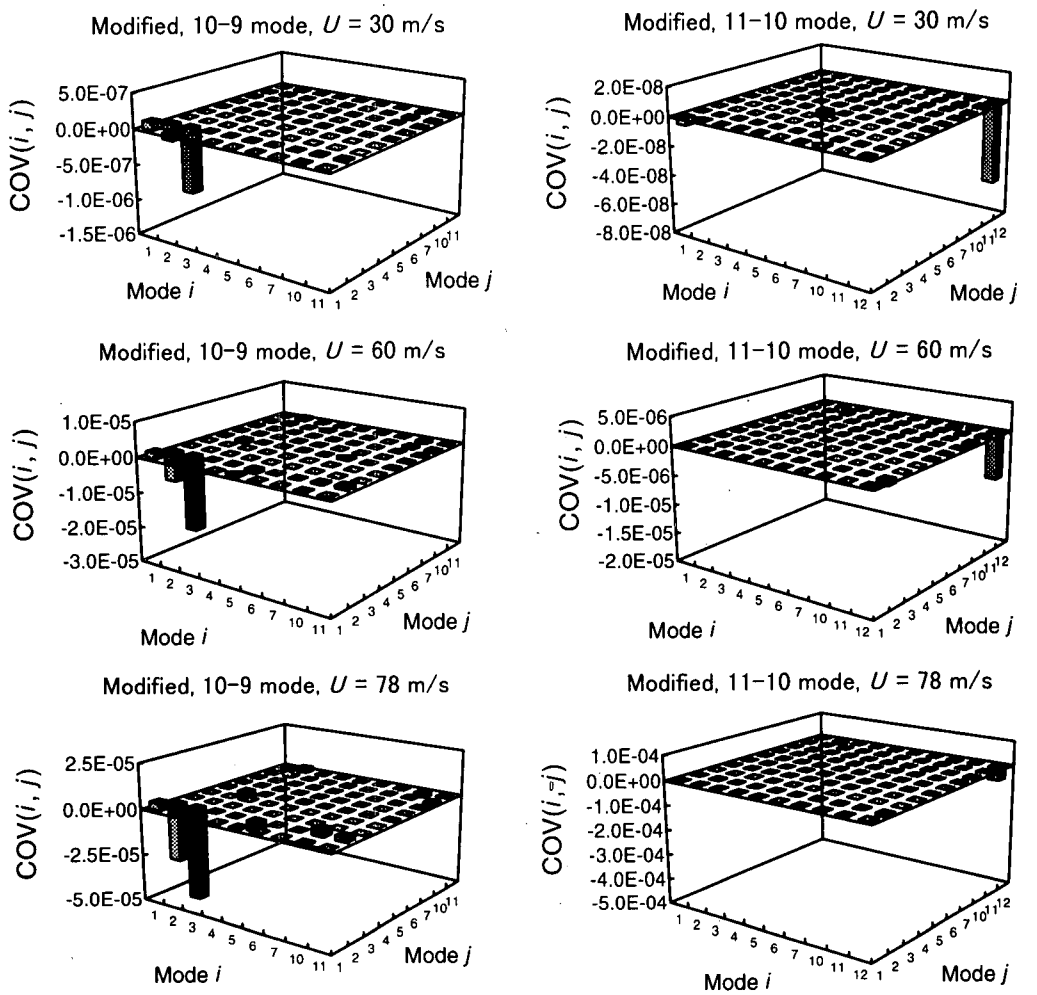

Fig. 8 Differences of COV matrices between 9- and 10-mode, and 10- and 11-mode analyses (Modified cross section)

parameter may be a primary reason for the reduction of the vertical RMS between the 9- and 10-mode analyses.

Thence, it is concluded that $G^{H_3^*}_{h_2\alpha_{12}}$ and $H_{h_2\alpha_{12}}$ contributed to the reduction of the vertical RMS in the 10-mode analysis, and they played a significant coupling role between modes 2 and 12. For the case of the reduction of the torsional RMS in the 11-mode analysis, examining the results in the same manner resulted in the observation that $G^{H_3^*}_{h_{13}\alpha_{12}}$ and $G^{A_1^*}_{\alpha_{12}h_{13}}$ contributed to the reduction of the torsional RMS in the 11-mode analysis, and they played a significant coupling role between modes 12 and 13.

It was noted earlier in the flutter section that H_3^* played a significant role in mode coupling even in buffeting. It can also be said that mode coupling between modes 2 and 12 is significant aeroelastically as well as aerodynamically, since the significance of $H_{h_2\alpha_{12}}$ was observed in the parameter analysis.

5. CONCLUSIONS

Analytical studies of mode coupling in the flutter and buffeting of the Akashi-Kaikyo Bridge were performed. The flutter analysis well predicted the flutter speed of the wind-tunnel model of the Akashi-Kaikyo Bridge. It also revealed multi-mode coupled flutter in which six primary modes; 1st symmetric vertical (mode 2) and torsion (mode 12),

Table 7 Parameter analyses for mode coupling in buffeting

(Original Cross Section, $\alpha_w = 0$ deg., $U = 60$ m/s)

	σ_h (m)	σ_α (deg.)	COV(ξ_i, ξ_j)
9-mode analysis	0.4874	—	COV(ξ_2, ξ_2) = 1.4037E-04
10-mode analysis	0.4522	0.6020	COV(ξ_2, ξ_2) = 1.1551E-04 COV(ξ_{12}, ξ_{12}) = 1.0974E-04
Parameter analyses for 10-mode analysis			
$G^{H_2^*}_{h_2\alpha_{12}} = 0$	0.4508	—	COV(ξ_2, ξ_2) = 1.1506E-04
$G^{H_3^*}_{h_2\alpha_{12}} = 0$	0.4878	—	COV(ξ_2, ξ_2) = 1.4099E-04
$G^{A_1^*}_{\alpha_{12}h_2} = 0$	0.4630	—	COV(ξ_2, ξ_2) = 1.2181E-04
$G^{A_4^*}_{\alpha_{12}h_2} = 0$	0.4552	—	COV(ξ_2, ξ_2) = 1.1534E-04
$H_{h_2\alpha_{12}} = 0$ [1]	0.4772	—	COV(ξ_2, ξ_2) = 1.3187E-04
$H_{h_2p_{12}} = 0$ [1]	0.4615	—	COV(ξ_2, ξ_2) = 1.2005E-04
11-mode analysis	—	0.5460	COV(ξ_{12}, ξ_{12}) = 0.9015E-04
Parameter analyses for 11-mode analysis			
$G^{H_2^*}_{h_{13}\alpha_{12}} = 0$	—	0.5519	COV(ξ_{12}, ξ_{12}) = 0.9213E-04
$G^{H_3^*}_{h_{13}\alpha_{12}} = 0$	—	0.5979	COV(ξ_{12}, ξ_{12}) = 1.0826E-04
$G^{A_1^*}_{\alpha_{12}h_{13}} = 0$	—	0.5966	COV(ξ_{12}, ξ_{12}) = 1.0779E-04
$G^{A_4^*}_{\alpha_{12}h_{13}} = 0$	—	0.5489	COV(ξ_{12}, ξ_{12}) = 0.9113E-04
$H_{h_{13}\alpha_{12}} = 0$ [1]	—	0.5440	COV(ξ_{12}, ξ_{12}) = 0.8949E-04
$H_{h_{13}p_{12}} = 0$ [1]	—	0.5460	COV(ξ_{12}, ξ_{12}) = 0.9015E-04

Note: 1)H-integral terms associated with S_{uu}, S_{ww} and C_{uw} were equated to zero.

and 2nd and 3rd vertical (modes 10 and 13) with less participation of 1st and 2nd lateral (modes 1 and 11), were coupled.

An investigation of the mechanism of mode coupling in flutter showed that the strong mode couplings were present in the diagonal component associated with mode 12 as well as off-diagonal components among modes 2, 10 or 13, and 12, and among modes 2, 10 and 13. This may be related to the fact that the flutter of the Akashi-Kaikyo Bridge was a bending-torsion coupled type and mode 12 was a dominant mode in flutter. Flutter derivatives introducing the strong mode couplings were H_1^*, H_2^* and P_2^* in $\mathbf{A}_{ij}$, and H_3^*, H_4^*, P_3^* and A_3^* in $\mathbf{B}_{ij}$.

The multi-mode buffeting analysis also well predicted the action of the wind-tunnel model of the Akashi-Kaikyo Bridge, particularly the nonlinear increment of the torsion observed in the high wind-speed region of 78 m/s due to mode coupling, which was never seen in the equivalent single-mode analysis. However, there remains the as-yet unexplained difference in the lateral response from both analytical methods between the analysis and measurements. Possible reasons for the difference are suggested as estimation errors associated with P_1^* and the representation of aerodynamic admittance. This is an important topic for continuing research and perhaps the availability of full-scale data may shed some light on this issue.

Significant mode couplings in the buffeting response were also recognized. Mode 12 suppressed vertical response and mode 13 suppressed torsional response. Those reductions were mainly due to the changes of diagonal components in the covariance matrix of the generalized coordinate; COV(ξ_2, ξ_2) and COV(ξ_{12}, ξ_{12}), respectively. The parameter study showed that $G^{H_3^*}_{h_2\alpha_{12}}$ and $H_{h_2\alpha_{12}}$ for the reduction of COV(ξ_2, ξ_2), and $G^{H_3^*}_{h_{13}\alpha_{12}}$ and $G^{A_1^*}_{\alpha_{12}h_{13}}$ for that of COV(ξ_{12}, ξ_{12}) played a significant coupling role.

ACKNOWLEDGMENT: The wind-tunnel test of the Akashi-Kaikyo Bridge was performed as a

cooperation study between Honshu-Shikoku Bridge Authority and Public Works Research Institute, Japanese Ministry of Construction. The test result was discussed at the technical committee for the wind-resistant design of the Honshu-Shikoku Bridges chaired by Dr. Toshio Miyata, Yokohama National University in Japan. The discussion in the committee was very helpful for this study.

REFERENCES

1) Miyata, T., Tada, K., Sato, H., Katsuchi, H. and Hikami, Y.: New Findings of Coupled-Flutter in Full Model Wind Tunnel Tests on the Akashi Kaikyo Bridge, *Proc. of Symp. on Cable-Stayed and Suspension Bridges*, Deauville, France, pp.163-170, 1994.
2) Chen, Z.Q.: The Three Dimensional Analysis of Behaviours Investigation on the Critical Flutter State of Bridges, *Proc. Symp. on Cable Stayed Bridges*, Shanghai, China, pp. 10-13, 1994.
3) Tanaka, H., Yamamura, N. and Shiraishi, N.: Multi-Mode Flutter Analysis and Two and Three Dimensional Model Tests on Bridges with Non-Analogous Modal Shapes, *J. Str. Mech. Earthquake Engrg.*, JSCE, Vol.10, No.2, July, pp.35-46, 1993.
4) Namini, A., Albrecht, P. and Bosch, H.: Finite Element-Based Flutter Analysis of Cable-Suspended Bridges, *J. Str. Engrg.*, ASCE, 118(6), pp.1509-1526, 1992.
5) Jones N.P., and Scanlan R.H.: Issues in the Multimode Aeroelastic Analysis of Cable-stayed Bridges, *Infrastructure '91, Intl. Workshop. on Tech. for Hong Kong's Infrastructure Development.*, Hong Kong, pp.281-290, 1991.
6) Lin, Y.K. and Yang, J.N.: Multimode Bridge Response to Wind Excitation, *J. Engrg. Mech. Div.*, ASCE, 109(2), pp.586-603, 1983.
7) Jain, A., Jones, N.P. and Scanlan, R.H.: Coupled Flutter and Buffeting Analysis of Long-Span Bridges, *J. Str. Engrg.*, ASCE. 122(7), pp.716-725, 1996.
8) Jain, A.: Multi-Mode Aeroelastic and Aerodynamic Analysis of Long-Span Bridges, *Thesis submitted in conformity with the requirements for Doctor of Philosophy*, The Johns Hopkins University, Baltimore, MD, USA, 1996.
9) Scanlan, R.H. and Jones, N.P.: Aeroelastic Analysis of Cable-Stayed Bridges, *J. Struct. Engrg.*, ASCE, 116(2), pp.279-297, 1990.
10) Jones, N.P., Jain, A. and Scanlan, R.H.: Multi-Mode Aerodynamic Analysis of Long-Span Bridges, *Proc. Str. Cong.*, ASCE, Atlanta, USA, pp.894-899, 1994.
11) Roberts, J.B. and Surry, D.: Coherence of Grid-Generated Turbulence, *Journal of Engrg. Hydraulics*, ASCE, 99(6), pp.1227-1245, 1973.
12) Honshu-Shikoku Bridge Authority and Bridge & Offshore Engineering Association: *Report on Full-Model Wind Tunnel Testing of the Akashi-Kaikyo Bridge: Results of Turbulent Flow Test*, 1992. (in Japanese)
13) Sato, H., Matsuno, H. and Kitagawa, M.: Measuring of Aerodynamic Admittance of the Akashi-Kaikyo Bridge, *Proc. of 13th Symposium of JAWE*, pp.131-136, 1994.
14) Kaimal, J.C., Wyngaard, J.C., Izumi, Y. and Cote, O.R.: Spectral Characteristics of Surface-Layer Turbulence, *Quart. J. Royal Met. Soc.*, 98, pp.563-589, 1972.
15) Honshu-Shikoku Bridge Authority and Ishikawajima-Harima Heavy Industries Co., Ltd.: *Report on Measurement of Flutter Derivatives of the Akashi-Kaikyo Bridge*, 1993. (in Japanese)
16) Singh, L., Jones, N.P., Scanlan, R.H. and Lorendeaux, O.: Identification of Lateral Flutter Derivatives of Bridge Decks, *J. of Wind Engrg. and Industrial Aerodynamics*, 60, pp.81-89, 1996.
17) Miyata, T. and Yamaguchi, K.: Aerodynamics of Wind Effects on the Akashi Kaikyo Bridge, *J. of Wind Engineering and Industrial Aerodynamics*, 48, pp.287-315, 1993.
18) Scanlan, R.H.: Amplitude and Turbulence Effects upon Bridge Flutter Derivatives, *J. Str. Engrg.*, ASCE, 123(2), pp.232-236, 1997.
19) Scanlan, R.H., Jones, N.P. and Lorendeaux, O.: Comparison of Taut-Strip and Section-Model-Based Approaches in Long-Span Bridge Aerodynamics', *Proc. of 9th Intl. Conf. on Wind Engrg.*, New Delhi, India, pp.950-961, 1995.
20) Katsuchi, H.: An Analytical Study on Flutter and Buffeting of the Akashi-Kaikyo Bridge, *Essay submitted in conformity with the requirements for Master of Science in Engineering*, The Johns Hopkins University, Baltimore, MD, USA, 1997.
21) Matsumoto, M., Hamasaki, H. and Yoshizumi, F.: On Flutter Stability of Decks for Super Long-Span Bridge, *J. of Structural Mechanics and Earthquake Engineering*, JSCE, No.537/I-35, pp.191-203, 1996. (in Japanese)

(Received September 5, 1997)

明石海峡大橋のフラッターとガスト応答におけるモード間連成の検討

勝地　弘・ジョーンズ ニコラス・スキャンラン ロバート・秋山晴樹

本論文は，明石海峡大橋のフラッターとガスト応答を対象に振動モード間の空力・構造連成を考慮した数値解析を行い，全橋模型風洞試験と比較するとともに，モード間連成について検討を行った結果を述べるものである．フラッター解析においては，6モードを用いることで模型で観測された顕著な連成効果を捉えることができるとともに，その連成メカニズムについて考察を加えた．また，ガスト応答解析においても鉛直たわみとねじれ変位に顕著なモード間連成の影響が認められ，その連成メカニズムについて考察を加えた．